Applied Catalysis A, General 550 (2018) 67–76

Contents lists available at ScienceDirect

Applied Catalysis A, General

journal homepage: www.elsevier.com/locate/apcata

Research Paper

Fabrication of mesoporous Co_3O_4 oxides by acid treatment and their catalytic performances for toluene oxidation

Genqin Li[a,b], Chuanhui Zhang[a,c,*], Zhong Wang[a], He Huang[a], Hui Peng[a], Xuebing Li[a,*]

[a] Key Laboratory of Biofuels, Qingdao Institute of Bioenergy and Bioprocess Technology, Chinese Academy of Sciences, Qingdao 266101, PR China
[b] University of Chinese Academy of Sciences, Beijing 100049, PR China
[c] Institute of Materials for Energy and Environment, School of Materials Science and Engineering, Qingdao University, Qingdao 266071, PR China

ARTICLE INFO

Keywords:
Toluene oxidation
Mesoporous Co_3O_4
Acid treatment
Surface acidity

ABSTRACT

Considering the harmful effects of volatile organic compounds (VOCs) on the atmosphere and public health, the search for proper catalytic materials for the effective catalytic elimination of VOCs remains one of the most pressing issues in the environmental field. In this study, a series of mesoporous Co_3O_4-n (n = 0.00, 0.0001, 0.01, 0.05, 0.10, 1.00, representing the concentration of HNO_3 aqueous solution) catalysts were fabricated by the acid treatment of Co_3O_4 that was previously prepared via a hydroxycarbonate precipitation method (Co_3O_4-P). The catalytic performances of the prepared catalysts were evaluated for the model reaction of toluene oxidation. An obvious enhancement of catalytic activity in the reaction was achieved over the acid-treated Co_3O_4 catalysts using lower HNO_3 concentrations, with Co_3O_4-0.01 exhibiting the optimum catalytic activity (T_{90} = 225 °C, 15 °C lower than that of Co_3O_4-P), excellent catalytic durability under dry conditions and a high regeneration capability under humid conditions. Benefitting from the dilute acid treatment, the Co_3O_4-n (n = 0.01, 0.05, 0.10) catalysts presented higher specific surface areas, more weak acidic sites and higher abundances of surface Co^{2+} and O_{ads} species, which were regarded as the key factors responsible for their enhanced catalytic activities.

1. Introduction

Volatile organic compounds (VOCs) emitted from industry and transport vehicles are recognized as major pollutants that are harmful to the atmosphere and human health. Among the various strategies proposed to eliminate VOCs, the catalytic oxidation of VOCs into harmless CO_2 and H_2O has been highlighted as one of the most effective pathways, with a low energy consumption and absence of secondary pollution. The focus of the catalytic oxidation of VOCs is the development of high-performance catalysts. Typically, supported noble metals are promising catalytic materials for VOCs oxidation. For example, supported platinum, palladium, gold and rhodium catalysts have been reported as efficient catalysts to remove VOCs at low temperature [1,2]. However, the disadvantages of these catalysts, such as high cost, easy-poisoning tendency and limited resources, hinder their wide industrial application. Alternatively, various transition metal oxides have been extensively studied over the past several years as oxidation catalysts because of their advantages including a lower price and adequate catalytic activities at relatively low temperature [3–10]. Among these metal oxides, Co_3O_4 has attracted much attention due to its excellent catalytic performance in numerous reactions, e.g., the catalytic oxidation of CO, NO or VOCs as well as soot combustion [11–18].

Considering that the process of reactant diffusion is a vital factor affecting the overall catalytic performance of a catalyst, a porous structure is anticipated to increase the amount of accessible active sites and improve the reactant-catalyst contact efficiency, thus enhancing the catalytic activity. For example, Dai's group found that mesoporous manganese and cobalt oxides exhibited better performance for the catalytic combustion of toluene/methanol/CO than their bulk counterparts [15,19,20]. Additionally, porous Co_3O_4 materials, synthesized by hydrothermal or microemulsion methods, facilitated the catalytic oxidation of toluene at relatively low temperatures [21]. Bruce's work also confirmed that mesoporous Co_3O_4, Cr_2O_3, Fe_2O_3, Mn_2O_3, and Mn_3O_4 catalysts exhibited high catalytic reactivity for CO oxidation [22]. Transition metal oxides are more susceptible to hydrolysis, redox or phase transition reactions, and they simultaneously possess different coordination modes as well as multiple oxidation states, hence, it is difficult to obtain their mesoporous structures [23–28]. Modified approaches such as the use of soft or hard templates, hydrothermal or microemulsion strategies have been reported for the synthesis of mesoporous materials [21,25,29–31]. However, these preparation processes are very complicated. Thus, it remains a great challenge to

* Corresponding authors at: Key Laboratory of Biofuels, Qingdao Institute of Bioenergy and Bioprocess Technology, Chinese Academy of Sciences, Qingdao 266101, PR China.
E-mail addresses: zhangch@qdu.edu.cn (C. Zhang), lixb@qibebt.ac.cn (X. Li).

http://dx.doi.org/10.1016/j.apcata.2017.11.003
Received 2 August 2017; Received in revised form 1 November 2017; Accepted 2 November 2017
Available online 03 November 2017
0926-860X/

prepare a catalyst with a mesoporous structure by simple methods [32,33].

Selective dissolution by an acid treatment is a common corrosion process in dealloying, in which an alloy is immersed into an acidic solution to remove the active element, leaving behind the inert element. Li and his coworkers introduced this technique for the treatment of three-dimensionally ordered macroporous $LaMnO_3$ perovskite with dilute HNO_3, acquiring a novel γ-MnO_2-like material after the selective removal of La cations [34]. This novel sample showed a significantly higher catalytic activity for CO oxidation than the initial precursor $LaMnO_3$ and ordinary γ-MnO_2 oxide, which was predominantly attributed to its large specific surface area and high degree of mesoporosity. Similarly, single or composite metal oxides have been reported to be post-treated by highly concentrated acid. For example, Sinha et al. synthesized mesoporous manganese oxide by a template-assisted method followed by chemical activation in 10 M sulfuric acid, which resulted in a large specific surface area and enhanced catalytic ability for VOCs oxidation at low temperature [35]. Additionally, it was also revealed that acid treatment can alter the valence states of metal ions in metal oxides, consequently modifying their catalytic activities. Askar et al. showed that manganese oxides with high valence states could be obtained through the formation of MnO_2 starting from Mn_2O_3 and Mn_3O_4 by acid activation, and hydrochloric acid tended to produce the so-called γ-MnO_2, while sulfuric acid produced α- or γ-MnO_2 [36].

In this work, a series of mesoporous Co_3O_4 catalysts were synthesized via a precipitation method with a subsequent acid treatment in dilute HNO_3 solutions, and their catalytic performances for toluene oxidation, which was chosen as the model reaction for VOCs abatement, were experimentally evaluated. Furthermore, these Co_3O_4 materials were extensively characterized by numerous techniques to better understand the impact of the acid treatment on their physicochemical properties, including the structure, morphology, porosity, redox ability, surface acidity and surface active species, thus revealing the structure-activity relationship. To the best of our knowledge, no previous work has reported the catalytic behaviors of acid-treated Co_3O_4 for the oxidation of VOCs.

2. Experimental

2.1. Catalyst preparation

All chemical reagents in the preparation process were of analytical grade, were purchased from the Sinopharm Chemical Reagent Co., Ltd. and were directly used without any further purification. Co_3O_4 oxide was prepared by a traditional precipitation method [16,37,38] with cobalt nitrate as the metal precursor and Na_2CO_3 aqueous solution as the precipitator. A 1.2 M Na_2CO_3 solution was added dropwise into a 0.5 M aqueous solution of cobalt nitrate under magnetic stirring until the pH value reached 8.5. After the solution was aged for 3 h at room temperature, the precipitate was collected and thoroughly washed with deionized water until the pH was 7. Then, the precipitate was dried at 110 °C in an oven overnight, followed by calcination at 500 °C for 4 h in a muffle furnace. The final obtained catalyst was denoted as Co_3O_4-P. Acid treatment was conducted by placing the starting Co_3O_4-P catalysts in HNO_3 aqueous solutions of different concentrations. Typically, each sample of Co_3O_4-P (6 g) was immersed into the HNO_3 solution (80 mL) with an acid concentration of 0.00 M (post-treated with deionized water), 0.0001 M, 0.01 M, 0.05 M, 0.10 M or 1.00 M. After the solution was stirred vigorously at room temperature for 10 h, the Co_3O_4 particles were collected, thoroughly washed with deionized water and dried at 110 °C overnight. Then, the obtained materials were calcined at 300 °C for 3 h in air. To facilitate the description below, the acid-treated Co_3O_4 catalysts were denoted as Co_3O_4-n (n = 0.00, 0.0001, 0.01, 0.05, 0.10 and 1.00, respectively, in terms of the HNO_3 concentration used for the Co_3O_4-P treatment).

2.2. Catalyst characterizations

Powder X-ray diffraction (XRD) patterns were collected on a Bruker D8 AVANCE diffractometer equipped with a monochromatic Cu Kα radiation source (λ = 1.5406 Å) in the range of 5–80° and operating at 40 kV and 30 mA. Scanning electron microscopy (SEM) analysis was conducted on a Hitachi E-1010 electron microscope at 200 kV. Nitrogen adsorption-desorption isotherms were measured on a Micromeritics ASAP2020 m + c apparatus at −196 °C. Prior to the measurement, all samples were degassed in a vacuum at 200 °C for 3 h. The specific surface area (S_{BET}) of each sample was obtained by the Brunauer-Emmett-Teller (BET) method and the pore volume and pore size distribution were calculated by the Barrett-Joyner-Halenda (BJH) method. X-ray photoelectron spectroscopy (XPS) measurements were performed on a Thermo Scientific ESCALAB 250Xi spectrometer using an Al Kα (1486.6 eV) radiation source at ambient temperature under a pressure typically on the order of 10^{-7} Pa. The binding energy (BE) was calibrated by utilizing C1s of adventitious carbon (284.8 eV) as a reference. The XPS spectra were deconvoluted using the XPS PEAK 41 program by curve fitting after Shirley-type background subtraction. Hydrogen temperature-programmed reduction (H_2-TPR) was performed using a Quantachrome Chembet Pulsar TPR/TPD apparatus with a thermal conductivity detector (TCD). The reducing gas was 10 vol.% H_2/Ar with a total flow rate of 50 mL min^{-1}, and the temperature range was from room temperature to 800 °C with a heating rate of 10 °C min^{-1}. The acidity of the Co_3O_4 catalysts was studied by ammonia temperature-programmed desorption (NH_3-TPD) on a Micromeritics 2920TR analyzer. In a typical experiment, 0.1 g of the catalyst was loaded in a flow quartz reactor and pretreated at 500 °C in Ar (10 mL min^{-1}) for 1 h. Afterwards, the sample was cooled to 100 °C under Ar flow, and ammonia adsorption was performed under a flow of 10 vol.% NH_3/Ar (40 mL min^{-1}) for 1 h. Subsequently, the catalyst was exposed to an Ar flow (10 mL min^{-1}) at 100 °C for 1 h to remove the physisorbed ammonia. TPD analysis was performed from 100 to 600 °C at a heating rate of 10 °C min^{-1} under a helium flow of 50 mL min^{-1}. The desorbed ammonia was quantitatively determined by the integration of the corresponding recorded profiles. A predefined volume of pure ammonia was used for the TCD calibration.

2.3. Catalytic testing

The catalytic activity of each Co_3O_4 catalyst for toluene oxidation was evaluated at atmospheric pressure in a continuous-flow fixed-bed tubular reactor (I.D. = 8 mm) under temperature-programmed operation. The catalyst (0.4 g, 60–80 mesh), diluted with an equal amount of quartz sand (0.4 g, 60–80 mesh) to minimize the effect of hot spots, was deposited on a quartz wool plug, and the reaction temperature of the catalyst bed was measured by a K-type thermocouple located within a concentric thermowell. Toluene vapor was generated by bubbling helium through a glass container of toluene chilled in an ice-water isothermal bath and completely mixed with two other O_2 and He streams with a total flow rate of 100 mL min^{-1} as the reaction feed (1000 ppm toluene vapor, 20 vol.% O_2 and He balance), which corresponded to a weight hourly space velocity (WHSV) of 15,000 mL g^{-1} h^{-1}. Prior to each evaluation, the reactor was heated from room temperature to 100 °C and maintained for 1 h to avoid the over estimation of toluene conversion (caused by adsorption). Afterwards, the reactor was continuously heated to 300 °C. The concentrations of toluene and other possible organic products were analyzed by an online Agilent 7890A gas chromatograph equipped with a flame ionization detector (FID) under a steady state. The toluene conversion ($X_{toluene}$%) was calculated based on the following equation:

$$X_{toluene}\% = \frac{[toluene]_{in} - [toluene]_{out}}{[toluene]_{in}} \times 100$$

where $[toluene]_{in}$ and $[toluene]_{out}$ represented the toluene

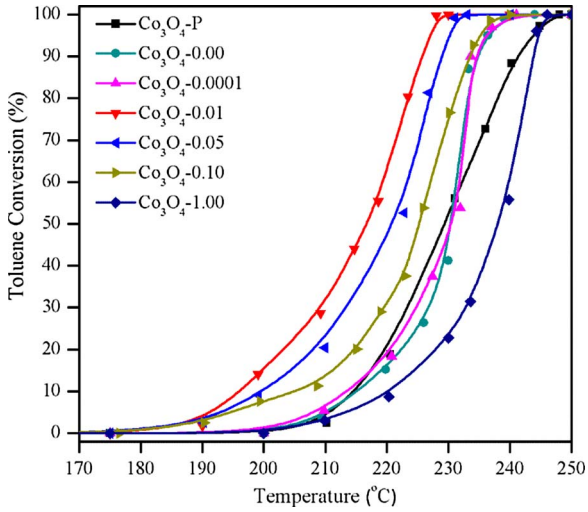

Fig. 1. Light-off curves of toluene conversion as a function of the reaction temperature over all Co_3O_4 catalysts.

concentrations in the inlet and outlet feeds, respectively.

3. Results and discussion

3.1. Catalytic performance

Firstly, a blank experiment was performed in the reactor loaded only with quartz sand. No significant toluene conversion was observed, indicating that there was no occurrence of a homogeneous reaction under the present reaction conditions. The light-off curves as a function of the reaction temperature over the prepared Co_3O_4-P and Co_3O_4-n (n = 0.00, 0.0001, 0.01, 0.05, 0.10 and 1.00) catalysts are shown in Fig. 1, and their catalytic activities are compared based on the values of T_{10}, T_{50} and T_{90} as well as the areal conversion rate (the molar quantity of converted toluene normalized per gram of catalyst and per specific surface area) at 210 °C, which are listed in Table 1. In terms of the combined results of Fig. 1 and Table 1, toluene conversion increased monotonously with the increase of the reaction temperature, which was beneficial from the catalytic effect of Co_3O_4 catalysts. The overall catalytic activities followed the sequence of Co_3O_4-0.01 > Co_3O_4-0.05 > Co_3O_4-0.10 > Co_3O_4-0.0001 ≈ Co_3O_4-0.00 > Co_3O_4-P > Co_3O_4-1.00 from the highest to the lowest. It was indicated that the concentration of the HNO_3 solution played a vital role in influencing the reaction activity of the obtained Co_3O_4-n catalyst. Relative diluted HNO_3 solutions (e.g. 0.0001, 0.01, 0.05, 0.10 and even 0.00 M) had positive effect on improving the activity of Co_3O_4-n catalysts for toluene oxidation, while HNO_3 solution of relatively high concentration (1.00 M) depressed the catalytic activity of Co_3O_4-1.00 catalyst. Among all catalysts, Co_3O_4-0.01 exhibited the optimum catalytic activity for toluene oxidation, while the Co_3O_4-1.00 catalyst suffered from excessive corrosion in the 1 M HNO_3 solution and exhibited the worst catalytic activity in the reaction. Additionally, the catalytic activity of Co_3O_4-0.00 is closely similar to that of Co_3O_4-0.0001, and both of them showed higher catalytic activities than Co_3O_4-P when the reaction temperature was above 230 °C. These results confirmed that treatment with dilute HNO_3 solutions (e.g. 0.0001, 0.01, 0.05, 0.10 and even 0.00 M) has a positive effect on the catalytic activities of Co_3O_4 catalysts, which resulted from their different physicochemical properties after the acid treatment. From the additional qualitative GC–MS analysis, CO_2 and H_2O were found to be the final products in the effluent, without any incomplete oxidation byproducts detected, which was attributed to the excellent oxidation reactivity of Co_3O_4 towards hydrocarbons, and a good carbon balance of 99.2% in each catalytic run was obtained. Additionally, Table 1 summarizes the catalytic activities for toluene oxidation over Co_3O_4-based (supported or unsupported) catalysts previously reported by other researchers. Despite the different reaction conditions, the prepared Co_3O_4-0.01 catalyst in this work presented an outstanding toluene oxidation activity, even compared with some supported noble metal catalysts. Thus, acid treatment with dilute HNO_3 solutions is an effective approach to improve the catalytic activity of Co_3O_4.

The catalytic stability of the best-performing Co_3O_4-0.01 catalyst was evaluated over 72 h under dry and humid conditions. As shown in Fig. 2A, toluene conversions of 90% and 60% remained constant without any deactivation under dry conditions at 225 and 218 °C during the overall testing period. Considering that water vapor usually exists in the exhaust from practical production and normally inhibits the catalytic activity of a catalyst for VOCs oxidation, it is reasonable to evaluate the catalytic endurance of Co_3O_4-0.01 under humid conditions. As shown in Fig. 2, the toluene conversion dropped from 90% to 85% with the addition of 3 vol.% water vapor, and it continuously decreased to 61% when a higher concentration (5 vol.%) of water vapor was fed into the stream. The above results suggested that the catalytic activity of the

Table 1
Catalytic activities for toluene oxidation over the prepared Co_3O_4 catalysts in this work and Co_3O_4-based catalysts previously reported by other researchers.

Catalysts	Catalytic activity				Ref.
	T_{10} (°C)	T_{50} (°C)	T_{90} (°C)	Areal conversion rate[a]	
Co_3O_4-P	215	229	241	3.2	This work[b]
Co_3O_4-0.00	215	230	235	–	This work
Co_3O_4-0.0001	213	231	235	–	This work
Co_3O_4-0.01	196	217	226	8.1	This work
Co_3O_4-0.05	199	221	229	6.4	This work
Co_3O_4-0.10	205	225	233	4.4	This work
Co_3O_4-1.00	220	238	244	2.2	This work
Co_3O_4 microspheres	240	266	285		[11][c]
7.4Au/Co_3O_4 microspheres	155	242	250		[11]
Co_3O_4-SBA16	206	232	240		[15][d]
Co_3O_4-KIT6	203	228	233		[15]
3DOM Co_3O_4	252	277	294		[41][e]
0.99Au/3DOM Co_3O_4	244	268	275		[41]
0.99Pd/3DOM Co_3O_4	180	206	218		[41]

[a] Areal conversion rate in units of 10^8 $mol_{toluene}$ m^{-2} s^{-1} under the reaction conditions at the reaction temperature of 210 °C.
[b] Under the conditions of the total flow rate of the reactant mixture [1000 ppm toluene + O_2 + He (balance)] = 100 mL min^{-1} and WHSV = 15,000 mL g^{-1} h^{-1}.
[c] Under the conditions of the total flow rate of the reactant mixture [1000 ppm toluene + O_2 + N_2 (balance)] = 16.7 mL min^{-1} and WHSV = 20,000 mL g^{-1} h^{-1}.
[d] Under the conditions of the total flow rate of the reactant mixture [1000 ppm toluene + O_2 + N_2 (balance)] = 33.3 mL min^{-1} and WHSV = 20,000 mL g^{-1} h^{-1}.
[e] Under the conditions of the total flow rate of the reactant mixture [1000 ppm toluene + O^2 + N^2 (balance)] = 33.4 mL min^{-1} and WHSV = 40,000 mL g^{-1} h^{-1}.

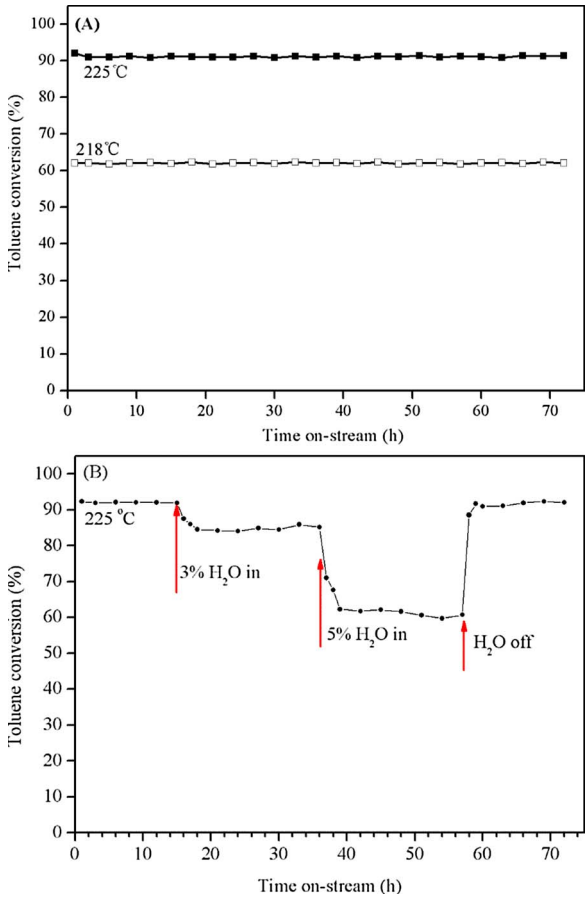

Fig. 2. Toluene conversion as a function of time on-stream over the Co_3O_4-0.01 catalyst: (A) dry conditions at 218 and 225 °C, respectively and (B) humid conditions at 225 °C.

Co_3O_4-0.01 catalyst was inhibited by water vapor due to the competitive adsorption of water and toluene molecules onto the active sites. After the removal of water vapor, the toluene conversion recovered, indicating the good regeneration ability of the Co_3O_4-0.01 catalyst.

3.2. Textural properties of Co_3O_4 catalysts

The XRD patterns of the Co_3O_4 catalysts are shown in Fig. 3. By referring to the Powder Diffraction Files (PDFs) of the Joint Committee on Powder Diffraction Standards (JCPDS), it was found that the characteristic peaks of all Co_3O_4 catalysts were in accordance with those of

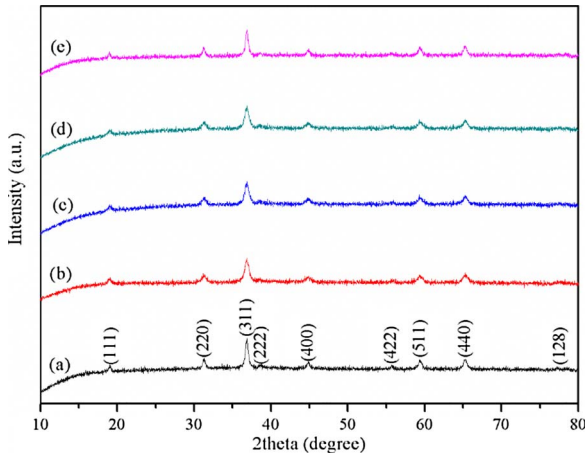

Fig. 3. XRD patterns of the Co_3O_4 catalysts: (a) Co_3O_4-P, (b) Co_3O_4-0.01, (c) Co_3O_4-0.05, (d) Co_3O_4-0.10 and (e) Co_3O_4-1.00.

Table 2
Textural properties of the Co_3O_4 catalysts.

Catalyst	Specific surface area ($m^2\,g^{-1}$)	Pore volume ($cm^3\,g^{-1}$)	Average pore size (nm)	D_{Co3O4}[a] (nm)
Co_3O_4-P	26	0.12	18.9	21.5 ± 0.9
Co_3O_4-0.01	72	0.16	8.9	13.8 ± 0.2
Co_3O_4-0.05	67	0.17	10.0	14.9 ± 0.4
Co_3O_4-0.10	56	0.16	11.0	19.7 ± 0.3
Co_3O_4-1.00	28	0.15	21.9	20.0 ± 0.3

[a] Average data calculated by the Scherrer equation based on the full width at half maximum (FWHM) of the XRD peaks (220, 311, 422, 511) over each catalyst.

cobalt oxide (JCPDS PDF# 42-1467) with a typical spinel crystal structure, and no reflection signal assignable to CoO or other phases was observed. The diffraction peaks at 2θ = 19.5, 31.6, 37.0, 39.0, 45.0, 56.3, 59.5, 65.5, and 77.9° corresponded to the crystalline planes of (111), (220), (311), (222), (400), (422), (511), (440), and (128), respectively, which was consistent with the results previously reported by other researchers [11,38–42]. These findings indicated that the acid treatment caused no obvious changes in the crystal structure of the Co_3O_4 catalyst. However, the diffraction peaks of the Co_3O_4 catalysts after acid treatment had a lower intensity and broader width, suggesting the lower degree of crystallinity and smaller crystalline sizes of the catalysts. Indeed, the average crystalline size (D_{Co3O4}) over each catalyst, which was calculated by the Scherrer equation (Table 2), shows that the value decreased from 21.5 nm for Co_3O_4-P to 13.8 nm for Co_3O_4-0.01, 14.9 nm for Co_3O_4-0.05, 19.7 nm for Co_3O_4-0.10 and 20.0 nm for Co_3O_4-1.00. Among all of the catalysts, the Co_3O_4-0.01 and Co_3O_4-0.05 catalysts had much smaller crystalline sizes, revealing a significant modification effect on the textural properties by treatment with a dilute acid solution.

The morphologies and structural features of the as-prepared Co_3O_4 catalysts were characterized by SEM. As shown in Fig. 4, the Co_3O_4-P catalyst presented a rough microblock morphology with a particle size of approximately 1.0-1.5 μm, and each microblock was disorderedly composed of granular aggregated entities with an average size of 22 nm (Fig. 4a and b). The acid treatment resulted in apparent and varied morphological changes over the Co_3O_4-n catalysts depending on the concentration of the HNO_3 solution. The Co_3O_4-n (n = 0.01, 0.05, 0.10) catalysts, which suffered slight corrosion with low HNO_3 concentrations (0.01 M, 0.05 M and 0.10 M), exhibited smoother microblock surfaces with uniform particle sizes of approximately 0.5–2.0 μm, and each microblock was constructed of an ordered aggregation of granular entities with an average size of 14–20 nm (Fig. 4c–h). Additionally, the treatment with higher concentration of a HNO_3 solution may lead to a more obvious rough surface morphology. For example, Co_3O_4-0.01 presented the smoothest bulk surface with a uniform structure, while a rough surface with numerous particle gaps was clearly observed on the Co_3O_4-0.10 catalyst. Eventually, as shown in Fig. 4i–j, the rough microblocks of Co_3O_4-P crumbled into small irregular particles after the treatment with 1.0 M HNO_3. In conclusion, the acid treatment proved to be an effective strategy for the morphological decoration of the Co_3O_4-P catalyst, in which the acid concentration plays a vital role in the decoration process.

The N_2 adsorption–desorption isotherms and pore-size distributions of the Co_3O_4 catalysts are shown in Fig. 5. Fig. 5A shows that all of the Co_3O_4 catalysts exhibited type IV isotherms with an obvious hysteresis phenomenon, indicating the presence of mesoporous structures in these catalysts [43–45]. In contrast, the hysteresis loops of the Co_3O_4-P and Co_3O_4-1.00 catalysts were located in the relative pressure (p/p_0) range of 0.8–1.0, which were much smaller than those of Co_3O_4-n (n = 0.01, 0.05, 0.10) with a different location in the relative pressure (p/p_0) range of 0.6-1.0. These differences may be caused by their various porous structures [46,47]. As shown in Table 2, the Co_3O_4-n (n = 0.01, 0.05, 0.10) catalysts had higher specific surface areas than Co_3O_4-P and

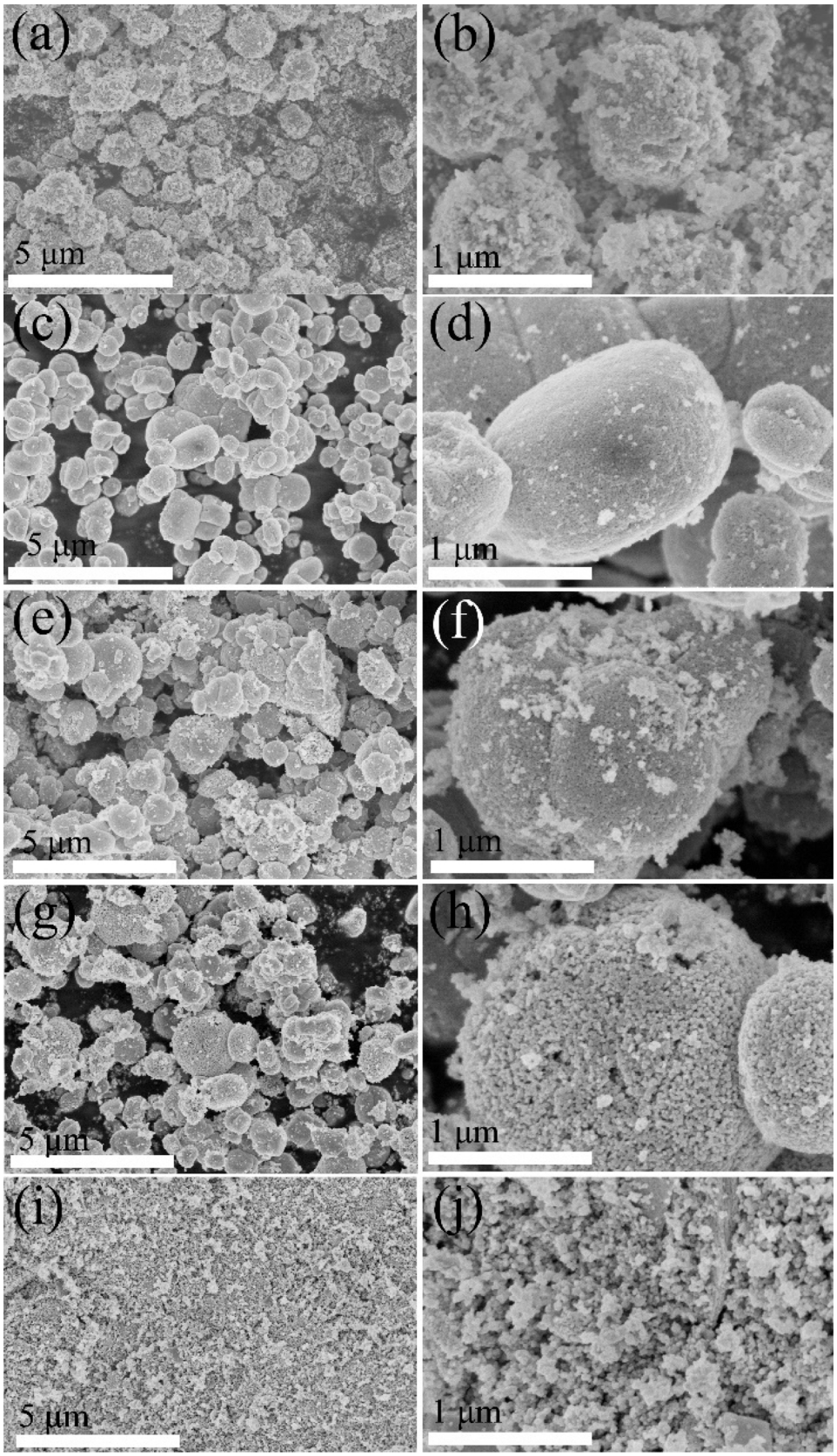

Fig. 4. SEM images of the Co_3O_4 catalysts: (a-b) Co_3O_4-P, (c-d) Co_3O_4-0.01, (e-f) Co_3O_4-0.05, (g-h) Co_3O_4-0.10 and (i-j) Co_3O_4-1.00.

Co_3O_4-1.00, which could be due to the formation of interparticle voids after the acid treatment [48]. Among all, Co_3O_4-0.01 had the highest specific surface area of 72 $m^2\ g^{-1}$, which beneficially originated from its smooth morphology, uniform structure and nanoparticle composition. According to the BJH pore size distributions of the Co_3O_4 catalysts in Fig. 5B, it can be noted that both Co_3O_4-P and Co_3O_4-1.00 exhibited broader pore size distributions in the overall range of 2–40 nm despite their mesoporous frameworks, while the Co_3O_4-n

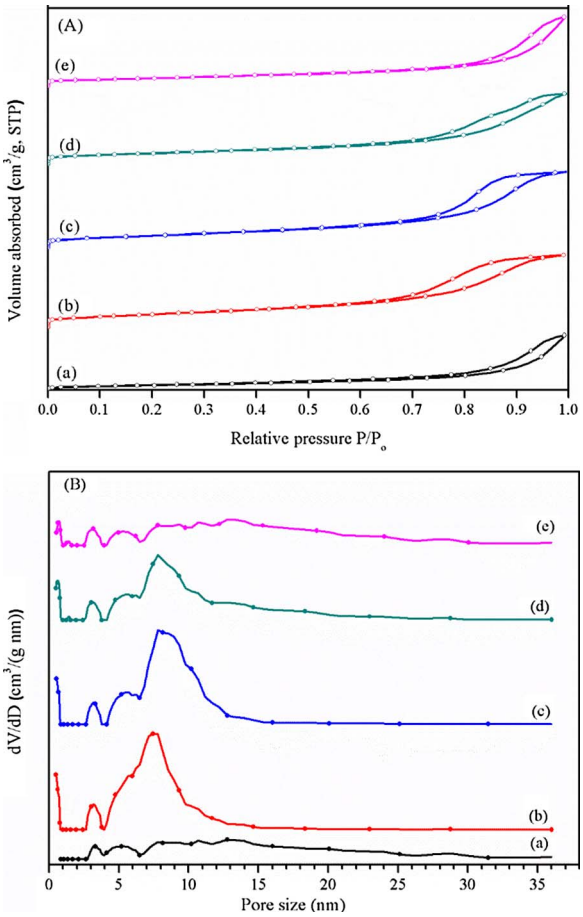

Fig. 5. (A) N_2 adsorption-desorption isotherms and (B) pore-size distributions of the Co_3O_4 catalysts: (a) Co_3O_4-P, (b) Co_3O_4-0.01, (c) Co_3O_4-0.05, (d) Co_3O_4-0.10 and (e) Co_3O_4-1.00.

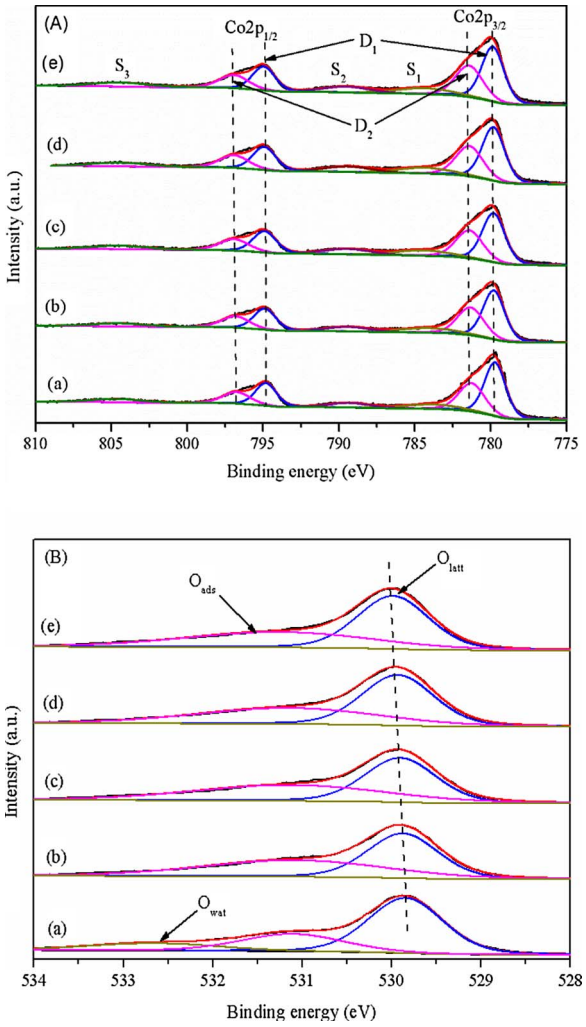

Fig. 6. (A) Co2p and (B) O1s XPS spectra of the Co_3O_4 catalysts: (a) Co_3O_4-P, (b) Co_3O_4-0.01, (c) Co_3O_4-0.05, (d) Co_3O_4-0.10 and (e) Co_3O_4-1.00.

(n = 0.01, 0.05, 0.10) catalysts showed analogous pore size distributions that were mostly centered in the range of 4–15 nm, indicating that the amorphous mesoporous structures of Co_3O_4 were effectively regulated and uniformed after the treatment with dilute acid. These results derived from the N_2 sorption were consistent with the information revealed from their SEM images. Moreover, the ordered porous structures of Co_3O_4-n (n = 0.01, 0.05, 0.10) were expected to be beneficial for the reactants diffusion and the facile accessibility to the active sites [49].

3.3. Surface elemental compositions, metal oxidation states and oxygen species

XPS measurements were performed to investigate the surface elemental compositions, metal oxidation states and adsorbed oxygen species of the prepared Co_3O_4 catalysts, and the corresponding Co2p and O1s XPS spectra are shown in Fig. 6. In Fig. 6A, the Co2p spectra of the Co_3O_4 catalysts were deconvoluted into two spin-orbit doublets, namely D1 and D2, and three satellite peaks, namely S1, S2, and S3, based on the following constraints: equal width for the two peaks of each doublet, equal width for the two smaller satellite lines (S1 and S2), and width of the most intense satellite peak (S3) fixed to 8.5 eV. The appearance of all these peaks revealed that both Co^{2+} and Co^{3+} coexisted in the prepared catalysts. As previously reported, the D1 doublet with a 2p level binding energy (BE) of 779.7–779.9 eV and a $2p_{3/2}$-$2p_{1/2}$ splitting of 15.1 eV was assigned to the octahedral Co^{3+}, while D2 with a 2p level BE of 781.3–781.4 eV and a $2p_{3/2}$-$2p_{1/2}$ splitting of 15.5 eV corresponded to the tetrahedral Co^{2+} [50]. The molar ratios of surface Co^{2+}/Co^{3+} are determined based on the fitting of XPS spectra and are listed in Table 3. The molar ratios of Co^{2+}/Co^{3+} over Co_3O_4 catalysts varied in the range of 0.67-0.77, indicating that Co^{3+} cations were the dominant species in Co_3O_4 spinel oxide. Additionally, the molar ratio of Co^{2+}/Co^{3+} from the highest to the lowest followed the sequence of Co_3O_4-0.01 (0.77) > Co_3O_4-0.05 (0.76) > Co_3O_4-0.10 (0.70) > Co_3O_4-1.00 (0.69) > Co_3O_4-P (0.67). It should be especially noted that the surface Co^{2+}/Co^{3+} molar ratios over the Co_3O_4-n catalysts were higher than that of Co_3O_4-P, revealing that certain amounts of Co^{3+} were transformed into Co^{2+} during the acid treatment, and consequently, more Co^{2+} species were present in the resulting Co_3O_4 materials. In Fig. 6B, a broad and asymmetrical O1s XPS spectrum is identified for each Co_3O_4 catalyst, which is mainly deconvoluted into two peaks corresponding to the existence of different surface oxygen species. The peaks at the BE of 529.8–530.0 eV and 531.1–531.2 eV could be attributed to the surface lattice oxygen (O_{latt}, i.e., O^{2-}) and adsorbed oxygen (O_{ads}, i.e., O_2^-, O_2^{2-} or O^-), respectively. In particular, the additional peak at 533.5 eV over Co_3O_4-P was characteristic of the oxygen species in surface adsorbed water [51,52]. As shown in Table 3, the surface O_{ads}/O_{latt} molar ratios remarkably increased over the Co_3O_4 catalysts after acid treatment compared with that of Co_3O_4-P, following the order of Co_3O_4-0.01 (0.96) > Co_3O_4-0.05 (0.90) > Co_3O_4-0.1 (0.80) > Co_3O_4-1.00 (0.76) > Co_3O_4-P (0.43).

3.4. Reducibility and acidity

Considering that the reducibility of a metal oxide catalyst is an important factor influencing its related catalytic performance in redox-

Table 3
Surface elemental compositions, reducibility and acidity of the Co_3O_4 catalysts.

Catalysts	Co^{2+}/Co^{3+} [a]	O_{ads}/O_{latt} [a]	Relative percentage of low-temperature H_2 consumption (%) [b]	Total amounts of acidic sites (mmol g^{-1}) [c]	Amounts of weak acidic sites (mmol g^{-1}) [c]	Amounts of strong acidic sites (mmol g^{-1}) [c]
Co_3O_4-P	0.67	0.43	25.8	0.105	0.072	0.033
Co_3O_4-0.01	0.77	0.96	22.1	0.350	0.123	0.227
Co_3O_4-0.05	0.76	0.90	23.4	0.324	0.109	0.215
Co_3O_4-0.10	0.70	0.80	24.0	0.308	0.102	0.206
Co_3O_4-1.00	0.69	0.76	24.7	0.217	0.071	0.146

[a] The data were determined from XPS spectra.
[b] The data were quantitatively estimated from H_2-TPR profiles.
[c] The data were quantitatively estimated from NH_3-TPD profiles.

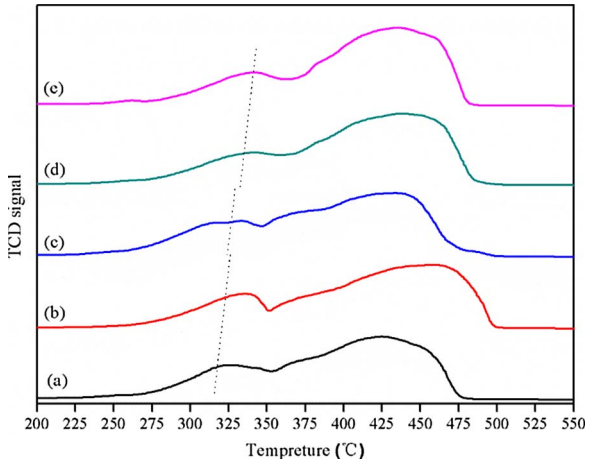

Fig. 7. H_2-TPR profiles of the Co_3O_4 catalysts: (a) Co_3O_4-P, (b) Co_3O_4-0.01, (c) Co_3O_4-0.05, (d) Co_3O_4-0.10 and (e) Co_3O_4-1.00.

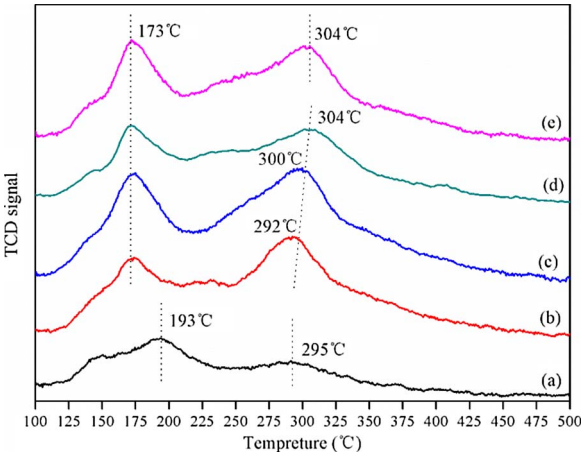

Fig. 8. NH_3-TPD profiles of the Co_3O_4 catalysts: (a) Co_3O_4-P, (b) Co_3O_4-0.01, (c) Co_3O_4-0.05, (d) Co_3O_4-0.10 and (e) Co_3O_4-1.00.

involving reactions [20], herein, H_2-TPR experiments were performed to investigate the reducibility of Co_3O_4 catalysts. The TPR profiles are presented in Fig. 7. Notably, there were mainly two reduction regions over the Co_3O_4 catalysts. The one in the low temperature range of 250–350 °C was attributed to the reduction of Co^{3+} into Co^{2+}, and the one in the high temperature range of 350–500 °C was associated with the further reduction of Co^{2+} to metallic cobalt [40]. The low-temperature reduction behaviors of Co_3O_4-0.01 and Co_3O_4-0.05 catalysts were similar to that of Co_3O_4-P in terms of their reduction temperature of peak maximums despite the different H_2 consumptions, which indicated that the low-temperature reducibility of Co_3O_4-P was minimally affected after the treatment with low-concentration HNO_3 (0.01 and 0.05 M). However, the temperature of the peak maximums in the low-temperature region over Co_3O_4-0.10 and Co_3O_4-1.00 shifted slightly towards higher orientation compared with that of Co_3O_4-P, meaning that a negative effect on the low-temperature reducibility was induced by the high-concentration acid treatment. Furthermore, more obvious and intensive high-temperature reduction regions could be observed over the acid-treated Co_3O_4 catalysts, which were possibly attributed to their increased Co^{2+} concentrations. According to the quantitative analysis of the overall TPR profiles, the relative percentage of low-temperature hydrogen consumption in the total consumption (%) over each catalyst was determined and is listed in Table 3, following a decreasing order of Co_3O_4-0.01 (22.1%) < Co_3O_4-0.05 (23.4%) < Co_3O_4-0.10 (24.0%) < Co_3O_4-1.00 (24.7%) < Co_3O_4-P (25.8%). These results implied the different distribution proportions of Co^{3+} and Co^{2+} in Co_3O_4 catalysts, and the treatment with lower acid concentrations tended to induce more transformations of Co^{3+} into Co^{2+}, which was in good agreement with the results of the surface Co^{2+}/Co^{3+} molar ratio from the XPS analysis.

The acidic properties of the prepared Co_3O_4 catalysts were explored by NH_3-TPD, and the recorded desorption profiles are presented in Fig. 8. It is well accepted that the temperature of the desorption peak maximum reflects the relative strength of the acidic sites, while the amount of desorbed ammonia determined from peak integration in the TPD profile corresponds to the quantity of relevant acidic sites [53–55]. Characteristically, there were two desorption peaks in the low and high temperature regions, corresponding to the weak and strong acidic sites on the surface, respectively. For Co_3O_4-P, the desorption signal of weak acidic sites was in the temperature range of 100–250 °C, and this signal consisted of a wide peak centered at 193 °C and a shoulder peak at 145 °C, while the signal of strong acidic sites had a low intensity with a broad peak centered at 295 °C in the temperature range of 250–500 °C. The low-temperature desorption profiles of the Co_3O_4-n (n = 0.01, 0.05, 0.10 and 1.00) catalysts were more obvious in the range of 100–210 °C, with intense peaks centered at 173 °C, indicating the presence of more weak acidic sites on the surface after the acid treatment of Co_3O_4-P. Additionally, the high-temperature profiles of the Co_3O_4-n catalysts had a stronger intensity than that of Co_3O_4-P, signifying the higher amounts of strong acidic sites on the surface as well. However, the temperatures of the peak maximums in this region varied depending on the specific catalyst from 292 to 304 °C, where the acid-treated Co_3O_4 using HNO_3 solutions of lower concentrations tended to present facile desorption behavior due to the higher abundance of strong acidic sites. In combination with the quantitative determination of the amounts of acidic sites (in units of mmol (NH_3) g^{-1}) in Table 3, the amounts of weak and strong acidic sites on the Co_3O_4-n catalysts significantly increased compared with those on Co_3O_4-P, resulting in higher total acidic quantities and giving a decreasing sequence of Co_3O_4-0.01 > Co_3O_4-0.05 > Co_3O_4-0.10 > Co_3O_4-1.00 > Co_3O_4-P.

3.5. Relationship between the physicochemical properties and catalytic activities

It has been accepted that the catalytic activity of a catalyst for VOCs oxidation can be greatly influenced by several factors, including the crystalline structure, specific surface area, porosity, reducibility and surface active species (i.e., surface-adsorbed oxygen or a metal cation redox couple) [20]. Additionally, it is also revealed that surface acidity may play a key role in hydrocarbon oxidation, which is attributed to the adsorption/oxidation behaviors of reactant molecules on the surface acidic sites [16,56].

In this work, the Co_3O_4-P and Co_3O_4-n catalysts exhibited typical spinel crystalline structures but varied catalytic performances, despite their different crystalline sizes, indicating no direct relation between the crystalline phases and the overall reactivity. Notably, compared with Co_3O_4-P and Co_3O_4-1.00, Co_3O_4-0.01, Co_3O_4-0.05 and Co_3O_4-0.10 possessed smooth microblock morphologies, ordered mesoporous structures and higher specific surface areas, increasing the reactant contact area and facilitating the diffusion of reactants and products [49]. These findings suggested that the textural properties including the porosity, specific surface area and surface morphology were successfully modified by acid treatment with relative diluted HNO_3 solutions, and these properties are thought to be an important factor influencing the catalytic activity.

According to the H_2-TPR results, it can be observed that the Co_3O_4-n catalysts exhibited similar low-temperature reduction behaviors to that of Co_3O_4-P despite the different hydrogen consumptions depending on the relative proportion of Co^{2+}/Co^{3+}, indicating the insignificant effect of low-temperature reducibility on the catalytic activity for toluene oxidation. The XPS results revealed that higher amounts of Co^{2+} were present on the surface of the acid-treated Co_3O_4-n catalysts, which may induce the formation of abundant oxygen vacancies in the formula of $Co_3O_{4-\delta}$. It is known that oxygen vacancies play a crucial role in the adsorption, activation and migration of oxygen species. As a result, the abundant surface oxygen vacancies may further increase the concentration of surface adsorbed oxygen, which was verified by the higher O_{ads} molar ratio in the XPS analysis. Accordingly, the abundance of surface Co^{2+} and O_{ads} as the active species for toluene oxidation is closely related with the total catalytic activity of the Co_3O_4 catalyst.

For the catalytic reaction of VOCs oxidation, the adsorption of VOCs molecules on the catalyst surface could also be of great importance. It has been shown that hydrocarbon oxidation could be initiated by the adsorption of hydrocarbons on the surface acidic sites of a catalyst by proton transfer [57,58], while the concentration and strength of surface acidic sites could influence the strength or extent of adsorption/oxidation of hydrocarbon molecules. Thus, the surface acidity of a catalyst may be another factor in VOCs oxidation. As indicated by NH_3-TPD, the acid treatment modified the acidity of Co_3O_4 catalysts, leading to higher acidic intensity and more abundant acidic sites. Indeed, compared with Co_3O_4-P, Co_3O_4-0.01, Co_3O_4-0.05 and Co_3O_4-0.10 catalysts had much higher concentrations of total acidic sites and especially considerable amounts of weak acidic sites, which probably resulted in the notable enhancement of their catalytic activities in the reaction.

To gain insights into the structure-activity relationship for the Co_3O_4 catalysts, an intuitive analysis was performed based on the correlated profiles of T_{50}, which was selected as a parameter for the evaluation of the catalytic activity, with the specific surface area (Fig. 9A), amount of weak acidic sites (Fig. 9B), surface Co^{2+} abundance (Fig. 9C) and surface O_{ads} abundance (Fig. 9D) over Co_3O_4-P and Co_3O_4-n catalysts. As shown in Fig. 9A, the T_{50} values for the Co_3O_4-P and Co_3O_4-n catalysts gradually decreased with an obvious increase in the specific surface area. However, the present results as well as other previously reported results revealed that the specific surface area may not be the only factor affecting the total catalytic activity of some catalyst. Indeed, the areal conversion rates of toluene in Table 1 over the catalysts varied following the order of Co_3O_4-0.01 > Co_3O_4-

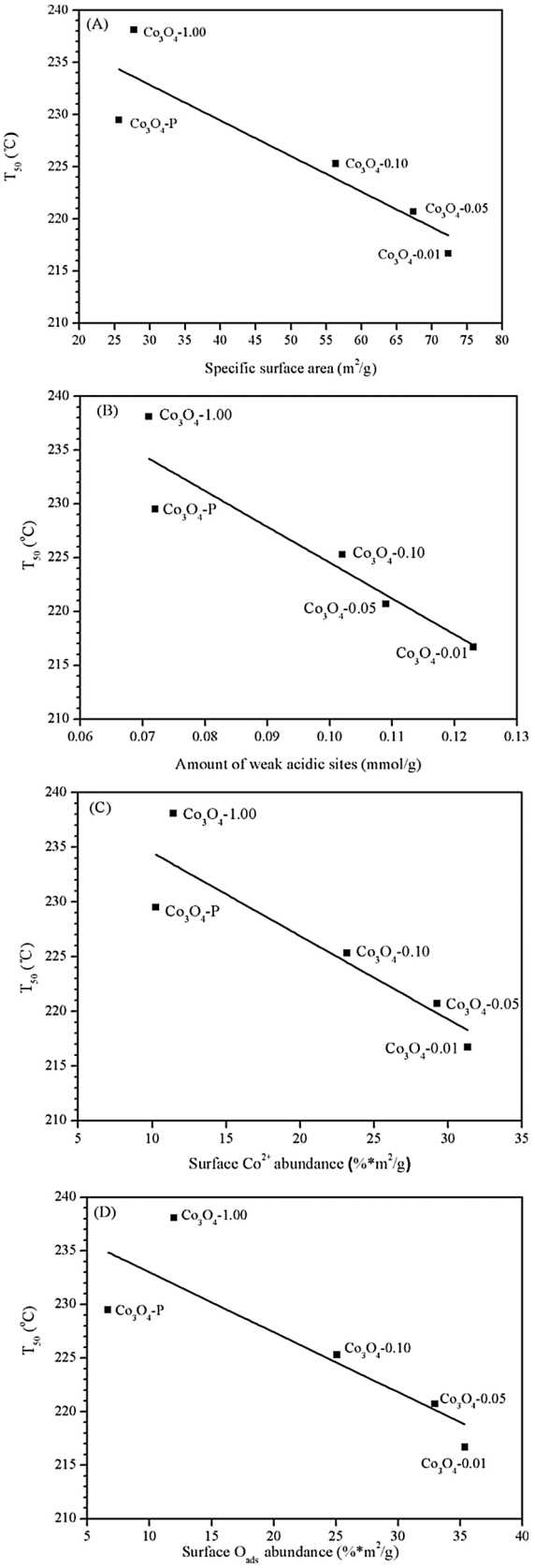

Fig. 9. The correlation of T_{50} with the (A) specific surface area, (B) amount of weak acidic sites, (C) surface Co^{2+} abundance and (D) surface O_{ads} abundance over Co_3O_4 catalysts.

0.05 > Co_3O_4-0.10 > Co_3O_4-P > Co_3O_4-1.00. The inconsistency in their areal conversion rates evidently implied that some other factors also played special roles in determining the overall catalytic activities of Co_3O_4 catalysts. As expected, the results in Fig. 9 B-D showed that the T_{50} values also gradually decreased with an obvious increase in the amount of weak acidic sites and surface Co^{2+} and O_{ads} abundances for the Co_3O_4-P, Co_3O_4-0.10, Co_3O_4-0.05 and Co_3O_4-0.01 catalysts, implying the good relationship of these three parameters with the catalytic activity for toluene oxidation. However, Co_3O_4-1.00 should be individually discussed due to its special behavior. Compared with Co_3O_4-P, Co_3O_4-1.00 had a similar specific surface area, weak acidity, surface Co^{2+} abundance and even higher surface O_{ads} abundance, but it showed an inhibited catalytic activity for toluene oxidation. This phenomenon could be attributed to the extremely irregular structure and powdered particles of Co_3O_4-1.00, as shown in Fig. 4i–j, which had a negative effect on the reactant adsorption, diffusion and oxidation. From this viewpoint, the overall catalytic activity of one Co_3O_4 catalyst in the reaction could originate from the synergistic effect of several factors including the textural properties, surface acidity and relative abundances of surface active species (Co^{2+}/Co^{3+} redox couple and O_{ads}).

4. Conclusions

A series of mesoporous Co_3O_4 catalysts (Co_3O_4-n, n = 0.00, 0.0001, 0.01, 0.05, 0.10 and 1.00) were independently synthesized by the treatment of Co_3O_4 that was previously prepared via a hydroxylcarbonate precipitation method with dilute HNO_3 solutions, and the catalytic oxidation of toluene as the model reaction was used to evaluate their catalytic performances. The results indicate that the catalytic activities of these Co_3O_4 catalysts decrease in the order of Co_3O_4-0.01 > Co_3O_4-0.05 > Co_3O_4-0.10 > Co_3O_4-0.0001 ≈ Co_3O_4-0.00 > Co_3O_4-P > Co_3O_4-1.00. Among all, Co_3O_4-0.01 exhibited the optimum catalytic activity, excellent catalytic durability under dry conditions and high regeneration capability under humid conditions. Beneficial from the acid treatment, the resulting Co_3O_4-n (n = 0.01, 0.05 and 0.10) catalysts presented typical mesoporous structures with smooth microblock morphologies and uniform particle sizes under the maintenance of spinel crystalline phases, resulting in great increase in the specific surface areas and pore volumes. Moreover, the Co_3O_4-n catalysts exhibited less low-temperature H_2 consumption, considerable amounts of weak acidic sites, and higher molar ratios of surface Co^{2+}/Co^{3+} and O_{ads}/O_{latt} compared with Co_3O_4-P, indicating the significant effect of acid treatment on the surface acidity and active species distribution. According to the thorough analysis of structure-activity relationship, it can be concluded that the higher catalytic activities of the Co_3O_4-n (n = 0.01, 0.05, 0.10) catalysts were basically associated with the higher specific surface area, larger amounts of weak acidic sites and more abundances of surface Co^{2+} and O_{ads} species. Thus, acid treatment with dilute HNO_3 solutions is an effective approach to fabricate mesoporous Co_3O_4 catalysts with unique physicochemical properties and superior catalytic activities.

Acknowledgements

We gratefully acknowledge the financial support from the National Natural Science Foundation of China (Nos. 21607163 and 21676287), the Natural Science Foundation of Shandong Province (Nos. ZR2016BQ02 and ZR2017ZC0633) and the Applied Basic Research Program of Qingdao (No. 16-5-1-35-jch).

References

[1] C.Y. Chen, X. Wang, J. Zhang, S.X. Pan, C.Q. Bian, L. Wang, F. Chen, X.J. Meng, X.M. Zheng, X.H. Gao, F.S. Xiao, Catal. Lett. 144 (2014) 1851–1859.
[2] T. Barakat, J.C. Rooke, H.L. Tidahy, M. Hosseini, R. Cousin, J.F. Lamonier, J.M. Giraudon, G. De Weireld, B. Su, S. Siffert, ChemSusChem 4 (2011) 1420–1430.
[3] N. Blanch-Raga, A.E. Palomares, J. Martinez-Triguero, S. Valencia, Appl. Catal. B: Environ. 187 (2016) 90–97.
[4] J.C. Hernandez-Garrido, D. Gaona, D.M. Gomez, J.M. Gatica, H. Vidal, O. Sanz, J.M. Rebled, F. Peiro, J.J. Calvino, Catal. Today 253 (2015) 190–198.
[5] B. Faure, P. Alphonse, Appl. Catal. B: Environ. 180 (2016) 715–725.
[6] S.D. Li, H.S. Wang, W.M. Li, X.F. Wu, W.X. Tang, Y.F. Chen, Appl. Catal. B: Environ. 166 (2015) 260–269.
[7] M. Romero-Saez, D. Divakar, A. Aranzabal, J.R. Gonzalez-Velasco, J.A. Gonzalez-Marcos, Appl. Catal. B: Environ. 180 (2016) 210–218.
[8] Y.J. Xie, Y. Guo, Y.L. Guo, L. Wang, W.C. Zhan, Y.S. Wang, X.Q. Gong, G.Z. Lu, RSC Adv. 6 (2016) 50228–50237.
[9] P.D. Yang, S.F. Zuo, Z.N. Shi, F. Tao, R.X. Zhou, Appl. Catal. B: Environ. 191 (2016) 53–61.
[10] M. Zawadzki, J. Okal, Catal. Today 257 (2015) 136–143.
[11] H.G. Yang, H.X. Dai, J.G. Deng, S.H. Xie, W. Han, W. Tan, Y. Jiang, C.T. Au, ChemSusChem 7 (2014) 1745–1754.
[12] W.Q. Song, A.S. Poyraz, Y.T. Meng, Z. Ren, S.Y. Chen, S.L. Suib, Chem. Mater. 26 (2014) 4629–4639.
[13] G. Salek, P. Alphonse, P. Dufour, S. Guillemet-Fritsch, C. Tenailleau, Appl. Catal. B: Environ. 147 (2014) 1–7.
[14] N. El Hassan, S. Aouad, S. Casale, H. El Zakhem, H. El Nakat, C. R. Chim. 17 (2014) 913–919.
[15] Y.C. Du, Q. Meng, J.S. Wang, J. Yan, H.G. Fan, Y.X. Liu, H.X. Dai, Microporous Mesoporous Mater. 162 (2012) 199–206.
[16] B. de Rivas, R. Lopez-Fonseca, C. Jimenez-Gonzalez, J.I. Gutierrez-Ortiz, J. Catal. 281 (2011) 88–97.
[17] T. Franken, R. Palkovits, Appl. Catal. B: Environ. 176–177 (2015) 298–305.
[18] T. Cai, H. Huang, W. Deng, Q.G. Dai, W. Liu, X.Y. Wang, Appl. Catal. B: Environ. 166 (2015) 393–405.
[19] J.G. Deng, L. Zhang, H.X. Dai, Y.S. Xia, H.Y. Jiang, H. Zhang, H. He, J. Phys. Chem. C 114 (2010) 2694–2700.
[20] Y.S. Xia, H.X. Dai, H.Y. Jiang, L. Zhang, Catal. Commun. 11 (2010) 1171–1175.
[21] G.M. Bai, H.X. Dai, J.G. Deng, Y.X. Liu, F. Wang, Z.X. Zhao, W.G. Qiu, C.T. Au, Appl. Catal. A: Gen. 450 (2013) 42–49.
[22] Y. Ren, Z. Ma, L.P. Qian, S. Dai, H.Y. He, P.G. Bruce, Catal. Lett. 131 (2009) 146–154.
[23] A. Rumplecker, F. Kleitz, E.-L. Salabas, F. Schüth, Chem. Mater. 19 (2007) 485–496.
[24] A.K. Sinha, K. Suzuki, Angew. Chem. Int. Ed. 44 (2005) 271–273.
[25] P.D. Yang, D.Y. Zhao, D.I. Margolese, B.F. Chmelka, G.D. Stucky, Nature 396 (1998) 152–155.
[26] A.K. Sinha, K. Suzuki, Appl. Catal. B: Environ. 70 (2007) 417–422.
[27] Y. Wang, C.M. Yang, W. Schmidt, B. Spliethoff, E. Bill, F. Schüth, Adv. Mater. 17 (2005) 53–56.
[28] J. Lee, M. Christopher Orilall, S.C. Warren, M. Kamperman, F.J. DiSalvo, U. Wiesner, Nat. Mater. 7 (2008) 222–228.
[29] Y.J. Zhang, L. Zhang, J.G. Deng, H.X. Dai, H. He, Inorg. Chem. 48 (2009) 2181–2192.
[30] F. Wang, H.X. Dai, J.G. Deng, G.M. Bai, K.M. Ji, Y.X. Liu, Environ. Sci. Technol. 46 (2012) 4034–4041.
[31] G.M. Bai, H.X. Dai, J.G. Deng, Y.X. Liu, W.G. Qiu, Z.X. Zhao, X.W. Li, H.G. Yang, Chem. Eng. J. 219 (2013) 200–208.
[32] Y. Wang, H. Xia, L. Lu, J.Y. Lin, ACS Nano 4 (2010) 1425–1432.
[33] S.-W. Bian, Y.-L. Zhang, H.-L. Li, Y. Yu, Y.-L. Song, W.-G. Song, Microporous Mesoporous Mater. 131 (2010) 289–293.
[34] W.Z. Si, Y. Wang, Y. Peng, J.H. Li, Angew. Chem. Int. Ed. 54 (2015) 7954–7957.
[35] A.K. Sinha, K. Suzuki, M. Takahara, H. Azuma, T. Nonaka, N. Suzuki, N. Takahashi, J. Phys. Chem. C 112 (2008) 16028–16035.
[36] M. Askar, H. Abbas, J. Power. Sources 51 (1994) 319–330.
[37] D. Pope, D.S. Walker, R.L. Moss, J. Catal. 47 (1977) 33–47.
[38] Q. Liu, L.-C. Wang, M. Chen, Y. Cao, H.-Y. He, K.-N. Fan, J. Catal. 263 (2009) 104–113.
[39] B. Bai, H. Arandiyan, J. Li, Appl. Catal. B: Environ. 142 (2013) 677–683.
[40] B. Solsona, T.E. Davies, T. Garcia, I. Vazquez, A. Dejoz, S.H. Taylor, Appl. Catal. B: Environ. 84 (2008) 176–184.
[41] T. Garcia, S. Agouram, J.F. Sanchez-Royo, R. Murillo, A. Maria Mastral, A. Aranda, I. Vazquez, A. Dejoz, B. Solsona, Appl. Catal. A: Gen. 386 (2010) 16–27.
[42] S.H. Xie, J.G. Deng, S.M. Zang, H.G. Yang, G.S. Guo, H. Arandiyan, H.X. Dai, J. Catal. 322 (2015) 38–48.
[43] F. Kleitz, F. Bérubé, R. Guillet-Nicolas, C.-M. Yang, M. Thommes, J. Phys. Chem. C 114 (2010) 9344–9355.
[44] B. Lee, D.L. Lu, J.N. Kondo, K. Domen, J. Am. Chem. Soc. 124 (2002) 11256–11257.
[45] W.B. Yue, A.H. Hill, A. Harrison, W.Z. Zhou, Chem. Commun. (2007) 2518–2520.
[46] C.Y. Ma, D.H. Wang, W.J. Xue, B.J. Dou, H.L. Wang, Z.P. Hao, Environ. Sci. Technol. 45 (2011) 3628–3634.
[47] C.Y. Ma, Z. Mu, J.J. Li, Y.G. Jin, J. Cheng, G.Q. Lu, Z.P. Hao, S.Z. Qiao, J. Am. Chem. Soc. 132 (2010) 2608–2613.
[48] Y.J. Zhang, L. Zhang, J.G. Deng, S.H. Xie, H.G. Yang, Y. Jiang, H.X. Dai, Proceedings of the 2014 International Conference on Materials Science and Energy Engineering (Cmsee 2014) (2015) 154–167.
[49] H. Tuysuz, M. Comotti, F. Schueth, Chem. Commun. (2008) 4022–4024.
[50] T.J. Chuang, C.R. Brundle, D.W. Rice, Surf. Sci. 59 (1976) 413–429.
[51] S. Ponce, M.A. Pena, J.L.G. Fierro, Appl. Catal. B: Environ. 24 (2000) 193–205.
[52] S. Rousseau, S. Loridant, P. Delichere, A. Boreave, J.P. Deloume, P. Vernoux, Appl. Catal. B: Environ. 88 (2009) 438–447.
[53] B. de Rivas, R. López-Fonseca, M.A. Gutiérrez-Ortiz, J.I. Gutiérrez-Ortiz, Appl.

Catal. B: Environ. 104 (2011) 373–381.
[54] A.L. Kustov, M.Y. Kustova, R. Fehrmann, P. Simonsen, Appl. Catal. B: Environ. 58 (2005) 97–104.
[55] S.S.R. Putluru, S. Mossin, A. Riisager, R. Fehrmann, Catal. Today 176 (2011) 292–297.
[56] S.A.C. Carabineiro, X. Chen, M. Konsolakis, A.C. Psarras, P.B. Tavares, J.J.M. Orfao, M.F.R. Pereira, J.L. Figueiredo, Catal. Today 244 (2015) 161–171.
[57] V.J. Fernandes Jr., A.S. Araujo, G.J.T. Fernandes, J. Therm. Anal. 56 (1999) 275–285.
[58] R. López-Fonseca, A. Aranzabal, J.I. Gutiérrez-Ortiz, J.I. Álvarez-Uriarte, J.R. González-Velasco, Appl. Catal. B: Environ. 30 (2001) 303–313.